Displacement and stress solutions for a viscoelastic half space subjected to a harmonic distributed tangential surface stress loading using the Radon and Fourier transforms

Marco Adolph, Euclides Mesquita
Depto. de Mecânica Computacional/FEM/UNICAMP, SP – Brazil
Edson R. Carvalho, Edivaldo Romanini
Depto. de Ciências Exatas, Centro Universitário de Três Lagoas, UFMS, MS – Brazil

Abstract

In this article a numerical solution for a 3D isotropic and viscoelastic half-space subjected to a rectangular tangential surface stress loading of constant amplitude is synthesized with the aid of the Radon and the Fourier integral transforms. The analysis is performed in the frequency domain, leading to a stationary solution. Viscoelastic effects are incorporated by means of the elastic-viscoelastic correspondence principle. The solution strategy makes use of the integral transform between the original spatial variables and the two-dimensional Radon transform. The equations of motion are analytically transformed to the Radon variables domain, resulting in a system of ordinary differential equations. The system of equations in the transformed Radon domain are solved for the given stress boundary conditions by means of the Fourier integral transform. The inverse Radon transform is performed analytically with respect to one of the variables and numerically with respect to the second variable. The inverse Fourier transform is performed numerically. A set of original solutions for the half-space under dynamic loading is reported in the article. The article also addresses the scheme used to perform the numerical inverse transformation.

Keywords: half space, viscoelasticity, Radon transform, Fourier transform, dynamic displacements and stresses

1 Introduction

The present work reports an effort to synthesize numerical solutions for 3D dynamic problems in unbounded domains. In another accompanying article [1] the case of a 3D viscoelastic half-space subjected to vertical rectangular loadings of constant amplitude has been described. In the present article the solution for the tangencial load is reported. These dynamic solutions for unbounded domains are important because they incorporate, in a natural way, the so-called Sommerfeld radiation condition

Mechanics of Solids in Brazil 2007, Marcílio Alves & H.S. da Costa Mattos (Editors)
Brazilian Society of Mechanical Sciences and Engineering, ISBN 978-85-85769-30-7

[2–4]. Domain type methods, like the Finite Element Method (FEM), require special formulations to model the radiation condition i.e., the withdrawal of energy from the system being analyzed by means of outgoing and non-reflected waves. These special schemes include the development of Infinite Elements [5, 6] or the implementation of the Dirichlet-to-Neumann (DtN) mapping at the outer boundary of the domain [7, 8]. On the other hand, the Boundary Element Method (BEM) can easily incorporate the Sommerfeld radiation condition, provided the auxiliary state used to transform the differential equations into boundary integral equations, also fulfill the radiation condition [9–11].

The development of these auxiliary dynamic solutions has drawn the attention of many researchers in the last three-decades. Surface displacement field of a three-dimensional viscoelastic half-space subjected to rectangular surface loading has been determined by Gaul [12] using the double Fourier integral transform. This non-singular displacement solution was incorporated into a superposition scheme to describe the dynamic interaction of surface foundations interacting with the soil, modeled as a half-space [13]. Two-dimensional half-space solutions for distributed loads using the Fourier integral transform have also been calculated by Rajapakse [14]. 2D solutions for anisotropic half-spaces and full-spaces with arbitrarily oriented principal directions have been reported in [15] also using the Fourier integral transform. Applications of the solutions developed in [15] to dynamic geomechanic problems have been reported in [16].

The In the last decade some articles reported the synthesis of full-space or half-space solutions using the Radon transform [17]. A fundamental solution for 3D anisotropic full-space using the Radon transform was presented by Wang and Achenbach [18]. In this article [18], the fundamental solutions for the 3D problem are given in terms of numerical integrations to be performed over a unit sphere. A numerical realization scheme for the full-space anisotropic solution was presented by Dravinski and Niu [19]. The solution of the three-dimensional problem of a concentrated load moving on the half-space surface was presented by Georgiadis and Lykotrafitis [20]. In article [20] the half-space solution is restricted to displacement fields determined at the half-space surface.

In the present work, stationary 3D displacement and stress fields are formulated using a solution strategy that applies both the Radon and the Fourier integral transforms [21]. The methodogy furnishes solutions for points at the half-space surface but also for points within the domain. The solution is validated by comparison with results computed with a procedure based on the double Fourier integral. The article also addresses the scheme used to perform the inverse transformations numerically. A set of original dynamic displacement solutions for points within the half-space are reported in the present article.

2 Problem statement

The problem to be solved consists of a 3D half space submitted to a tangential rectangular distributed load of constant amplitude with dimensions (2a x 2b) applied at the half-space free surface and presenting harmonic time behavior, see figure 1. The medium is considered isotropic and viscoelastic.

Mechanics of Solids in Brazil 2007, Marcílio Alves & H.S. da Costa Mattos (Editors)
Brazilian Society of Mechanical Sciences and Engineering, ISBN 978-85-85769-30-7

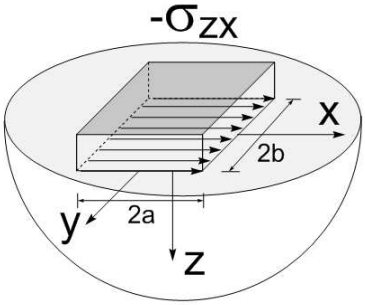

Figure 1: Half-space subjected to a tangential rectangular surface loading

The problem is governed by the Navier equations in the frequency domain which, in the absence of body forces, can be expressed in terms of the displacement components $\overline{U}_i\,(x,y,z,\omega)$ $(i=x,y,z)$as:

$$\mu\,\bar{U}_{i,jj}+(\lambda+\mu)\;\bar{U}_{j,ji}=-\omega^2\rho\bar{U}_i \tag{1}$$

In equation (1), μ and λ are Lamé constants, ρ is the continuum density and ω is the circular frequency. For linear isotropic continuum the components of the stress tensor $\overline{\sigma}_{ij}$ may be expressed in terms of the displacement components $\overline{U}_i$

$$\overline{\sigma}_{ij}=\mu\,(\bar{U}_{i,j}+\bar{U}_{j,i})+\delta_{ij}\lambda\,\bar{U}_{k,k} \tag{2}$$

In equation (2), δ_{ij} is the Kroenecker delta. The tangential traction excitation $\overline{\sigma}_{zx}\,(x.y.z=0,\omega)$ applied at the half-space surface $(z=0)$ is incorporated in the formulation as boundary conditions:

$$\overline{\sigma}_{zx}(x,y,z=0,\omega)\;=\begin{cases}-1; & |x|\le a,|y|\le b\\ 0 & ; \qquad |x|>a,|y|>b\end{cases} \tag{3}$$

$$\overline{\sigma}_{zy}(x,y,z=0,\omega)\;=0 \tag{4}$$

$$\overline{\sigma}_{zz}(x,y,z=0,\omega)\;=0 \tag{5}$$

Viscoelastic effects are introduced by means of the elastic-viscoelastic correspondence principle [22]. In applying this principle, the real Lamé constants μ, λ are substituted by complex valued parameters μ^*, λ^* containing the internal damping coefficient $\eta(\omega)$ in the imaginary part. In the present article the damping coefficient is considered constant, yielding the constant hysteretic damping model [22]:

$$\begin{cases}\lambda^*=\lambda\,[1+i\,\eta]\\ \mu^*=\mu\,[1+i\,\eta]\end{cases} \tag{6}$$

Mechanics of Solids in Brazil 2007, Marcílio Alves & H.S. da Costa Mattos (Editors)
Brazilian Society of Mechanical Sciences and Engineering, ISBN 978-85-85769-30-7

3 Solution strategy

The solution strategy applied in this article is a classical one. Initially, the displacement components of the Navier equations $\overline{U}_i\,(x,y,z,\omega)$ and the stress components at the half-space surface $\overline{\sigma}_{ix}\,(x,y,z=0,\omega)\quad (i=x,y,z)$ undergo a rotation of magnitude θ about the z-axis, relating the original $x-y$ axes to the primed $x'-y'$ axes. The primed axis x' is now coincident with the normal n, see figure 2. The definition of the Radon variables (s,θ) can also be seen in figure 2. After this coordinate rotation the Navier displacements (1) and the stress equations (2) may be expressed in terms of the primed axes components $\overline{U}_{i'}\,(x',y',z=z',\omega)$ and $\overline{\sigma}_{ix'}\,(x',y',z=z',\omega)$ with $(i'=x',y',z')$.

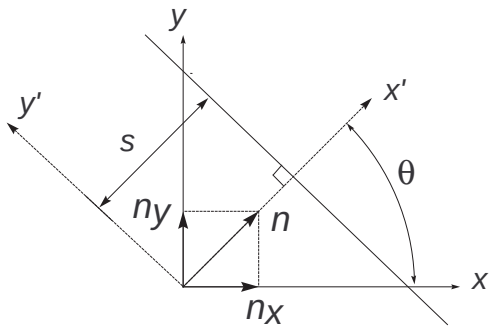

Figure 2: Scheme for coordinate rotation and Radon variables

In the second step the Navier equations written in the primed coordinate system (x',y',z') are transformed to the Radon domain variables with respect to the pair $(x',y'\leftrightarrow s,\theta)$, see [16, 21]. This transformation for isotropic media renders two uncoupled sets of partial differential equations in terms of the displacements in the Radon domain $\tilde{U}_{i'}\,(s,\theta,z=z',\omega)$, with $(i=x',y',z')$.

$$\left\{\mu\left[\frac{d^2}{ds^2}+\frac{d^2}{dz^2}\right]+\omega^2\rho\right\}\tilde{U}_{z'}+(\mu+\lambda)\left(\frac{d^2}{dsdz}\tilde{U}_{x'}+\frac{d^2}{dz^2}\tilde{U}_{z'}\right)=0 \tag{7}$$

$$\left\{\mu\left[\frac{d^2}{ds^2}+\frac{d^2}{dz^2}\right]+\omega^2\rho\right\}\tilde{U}_{x'}+(\mu+\lambda)\left[\frac{d^2}{ds^2}\tilde{U}_{x'}+\frac{d^2}{dsdz}\tilde{U}_{z'}\right]=0 \tag{8}$$

$$\left\{\mu\left[\frac{d^2}{ds^2}+\frac{d^2}{dz^2}\right]+\omega^2\rho\right\}\tilde{U}_{y'}=0 \tag{9}$$

The first two equations, (7) and (8), represent a two-dimensional coupled system in the Radon domain in terms of the displacement variables $\widetilde{U}_{x'}$ and $\widetilde{U}_{z'}$. Equation (9) in the variable $\widetilde{U}_{y'}$ is uncoupled from the two preceding ones. These two systems can be solved independently.

Solution of the two equation system. The first system, equations (7) and (8), can be solved with the aid of the Fourier transform, as can be found in [16]. A Fourier transform between the Radon

variable s and the Fourier variable k, is applied to these equations. The variable k represents a wave number. The solution in terms of the doubled transformed displacement variables $\hat{\tilde{U}}_{x'}(k,\theta,z,\omega)$ and $\hat{\tilde{U}}_{z'}(k,\theta,z,\omega)$ may be written as:

$$\hat{\tilde{U}}_{z'} = A\cdot e^{-\delta\alpha_1\cdot z} + B\cdot e^{\delta\alpha_1\cdot z} + C\cdot e^{-\delta\alpha_2\cdot z} + D\cdot e^{\delta\alpha_2\cdot z} \tag{10}$$

$$\hat{\tilde{U}}_{x'} = \psi_1 A\cdot e^{-\delta\cdot\alpha_1\cdot z} - \psi_1 B\cdot e^{\delta\cdot\alpha_1\cdot z} + \psi_2 C\cdot e^{-\delta\cdot\alpha_2\cdot z} - \psi_2 D\cdot e^{\delta\cdot\alpha_2\cdot z} \tag{11}$$

Analogously, the solutions for the surface stress components are expressed as:

$$\hat{\tilde{\sigma}}_{zz'}(k,\theta,z,\omega) = \Gamma_1 A e^{-\delta\alpha_1 z} - \Gamma_1 B e^{\delta\alpha_1 z} + \Gamma_2 C e^{-\delta\alpha_2 z} - \Gamma_2 D e^{\delta\alpha_2 z} \tag{12}$$

$$\hat{\tilde{\sigma}}_{zx'}(k,\theta,z,\omega) = \Gamma_3 A e^{-\delta\alpha_1 z} + \Gamma_3 B e^{\delta\alpha_1 z} + \Gamma_4 C e^{-\delta\alpha_2 z} + \Gamma_4 D e^{\delta\alpha_2 z} \tag{13}$$

In equations (10) and (11), a new variable δ, defined as $\delta = (\omega^2\rho)^{1/2}$, is introduced. The roots of the characteristic equation, α_1 and α_2 are given by [21]:

$$\alpha_1 = \sqrt{\frac{-c_3 - \sqrt{c_3^2 - 4c_1c_5}}{2c_1}} \quad ; \quad \alpha_2 = \sqrt{\frac{-c_3 + \sqrt{c_3^2 - 4c_1c_5}}{2c_1}} \tag{14}$$

With c_1, c_3 and c_5 being determined from the constitutive parameters λ, μ of the continuum and from a modified wave number variable, defined as $\xi = k/\delta$, [16, 21]:

$$c_{_1} = \lambda\mu + 2\mu^2 \tag{15}$$

$$c_{_3} = \left(-2\xi^2\lambda\mu - 4\xi^2\mu^2 + \lambda + 3\mu\right) \tag{16}$$

$$c_{_5} = \left(\xi^4\lambda\mu + 2\xi^4\mu^2 - \xi^2\lambda - 3\xi^2\mu + 1\right) \tag{17}$$

The expressions for ψ_1, ψ_2, Γ_1 to Γ_4 can be found in appendix A.

Solution of the second equation. The general solution for the uncoupled equation (9) follows essentially the same steps described in the previous section. The displacement and stress solution in the y'-direction is:

$$\hat{\tilde{U}}_{y'} = Ee^{-\beta\cdot\delta\cdot z} + Fe^{\beta\cdot\delta\cdot z} \tag{18}$$

$$\hat{\tilde{\sigma}}_{zy'} = -\mu\beta Ee^{-\beta\cdot\delta\cdot z} + \mu\beta Fe^{\beta\cdot\delta\cdot z} \tag{19}$$

with

$$\beta = \pm\sqrt{\frac{\mu\xi^2 - 1}{\mu}} \tag{20}$$

The integration constants A, B, C and D found in solutions (10) through (13) and the functions E and F present in equations (18) and (19) are to be determined from the boundary conditions.

4 Transformation of the boundary conditions to the Radon-Fourier domain.

In order to determine the constants present in the general solutions (10) to (13), (18) and (19) the boundary conditions given in equations (3) to (5) must also be transformed to the primed coordinate system, followed by a Radon transform with respect to the pair $(x', y' \leftrightarrow s, \theta)$ and a Fourier transform with respect to the variables $(s \leftrightarrow k)$ [21].

The algebraic manipulation is rather cumbersome [21] and the resulting surface stress boundary conditions in the transformed Radon-Fourier domain $\hat{\tilde{\sigma}}_{ix'}(k, \theta, z = 0, \omega)$ may be written as:

$$\hat{\tilde{\sigma}}_{zx'}(k, \theta, \omega, z = 0) = \hat{\tilde{\sigma}}_{zx}(k, \theta, \omega, z = 0)\cos\theta = -\frac{4}{\sqrt{2\pi}}\frac{\sin[\xi\delta a\cos(\theta)]\sin[\xi\delta b\sin(\theta)]}{(\xi\delta)^2\sin(\theta)\cos(\theta)}\cos\theta \tag{21}$$

$$\hat{\tilde{\sigma}}_{zy'}(k, \theta, \omega, z = 0) = -\hat{\tilde{\sigma}}_{zx}(k, \theta, \omega, z = 0)\sin\theta = +\frac{4}{\sqrt{2\pi}}\frac{\sin[\xi\delta a\cos(\theta)]\sin[\xi\delta b\sin(\theta)]}{(\xi\delta)^2\sin(\theta)\cos(\theta)}\sin\theta \tag{22}$$

$$\hat{\tilde{\sigma}}_{zz'}(k, \theta, \omega, z = 0) = 0 \tag{23}$$

Determination of the integration constants. It can be shown that to fulfill the Sommerfeld radiation condition, the functions B, D and F from equations (10), (13), (18) and (19) must vanish: $B = D = F = 0$. The values of A and C are determined by comparing the surface stress solutions (12) and (13) with the transformed boundary conditions (23) and (21), respectively. The value of E is obtained by applying condition (22) to equation (19). The results are:

$$A = \frac{\Gamma_2}{\Gamma_1\Gamma_4 - \Gamma_3\Gamma_2}\hat{\tilde{\sigma}}_{zx}\cos\theta = \frac{-4}{\sqrt{2\pi}}\frac{\Gamma_2}{\Gamma_1\Gamma_4 - \Gamma_3\Gamma_2}\frac{\sin[\xi\delta a\cos\theta]\sin[\xi\delta b\sin\theta]}{(\xi\delta)^2\sin\theta\cos\theta}\cos\theta \tag{24}$$

$$C = \frac{-\Gamma_1}{\Gamma_1\Gamma_4 - \Gamma_3\Gamma_2}\hat{\tilde{\sigma}}_{zx}\cos\theta = \frac{4}{\sqrt{2\pi}}\frac{\Gamma_1}{\Gamma_1\Gamma_4 - \Gamma_3\Gamma_2}\frac{\sin[\xi\delta a\cos\theta]\sin[\xi\delta b\sin\theta]}{(\xi\delta)^2\sin\theta\cos\theta}\cos\theta \tag{25}$$

$$E = -\hat{\tilde{\sigma}}_{zx}\frac{\sin\theta}{\mu\beta} = \frac{4}{\sqrt{2\pi}}\frac{\sin[\xi\delta a\cos\theta]\sin[\xi\delta b\sin\theta]}{(\xi\delta)^2\sin\theta\cos\theta}\frac{\sin\theta}{\mu\beta} \tag{26}$$

Expressions for the solutions in the original physical domain. Once the constants A, B, C, D, E and F are known, the problem is solved in the transformed Radon-Fourier domain. The remaining task is to transform the solutions back to the original physical domain. An inverse Fourier transform with respect to the pair $(k \leftrightarrow s)$ is applied to the solutions, followed by an inverse Radon transform with respect to the variables $(s, \theta \leftrightarrow x', y')$. A final coordinate rotation about the z-axis will bring the solution to the original (x, y, z, ω) domain.

The inverse Fourier and Radon transforms will produce two improper integrals over the variables k and s, as well as a proper integration with repect to the variable θ. It can be shown that the improper

integration with respect to the Radon variable s can be performed analytically [21]. After a long manipulation the final solution for displacements and stresses at the original domain are given by:

$$U_x(x,y,z,\omega) = \tfrac{1}{2\pi^2}\tfrac{1}{\sqrt{2\pi}} * \int_{-\pi/2}^{\pi/2}\int_{-\infty}^{\infty} \pi \cdot sign(\delta\xi)\, e^{i\delta\xi(x\cos\theta + y\sin\theta)} \xi\delta \left\{\cos\theta\left[\psi_1 A\cdot e^{-\delta\cdot\alpha_1\cdot z} + \psi_2 C\cdot e^{-\delta\cdot\alpha_2\cdot z}\right] - \sin\theta\left[E e^{-\beta\cdot\delta\cdot z}\right]\right\} d\xi d\theta \tag{27}$$

$$U_y(x,y,z,\omega) = \tfrac{1}{2\pi^2}\tfrac{1}{\sqrt{2\pi}} * \int_{-\pi/2}^{\pi/2}\int_{-\infty}^{\infty} \pi \cdot sign(\delta\xi)\, e^{i\delta\xi(x\cos\theta + y\sin\theta)} \xi\delta \left\{\sin\theta\left[\psi_1 A\cdot e^{-\delta\cdot\alpha_1\cdot z} + \psi_2 C\cdot e^{-\delta\cdot\alpha_2\cdot z}\right] + \cos\theta\left[E e^{-\beta\cdot\delta\cdot z}\right]\right\} d\xi d\theta \tag{28}$$

$$U_z(x,y,z,\omega) = \frac{1}{2\pi^2}\frac{1}{\sqrt{2\pi}} \int_{-\pi/2}^{\pi/2}\int_{-\infty}^{\infty} \pi \cdot sign(\delta\xi)\, e^{i\delta\xi(x\cos\theta + y\sin\theta)} \xi\delta \left\{A\cdot e^{-\delta\cdot\alpha_1\cdot z} + C\cdot e^{-\delta\cdot\alpha_2\cdot z}\right\} d\xi d\theta \tag{29}$$

$$\sigma_{zx}(x,y,z,\omega) = \tfrac{1}{2\pi^2}\tfrac{1}{\sqrt{2\pi}} * \int_{-\pi/2}^{\pi/2}\int_{-\infty}^{\infty} \pi \cdot sign(\delta\xi)\, e^{i\delta\xi(x\cos\theta + y\sin\theta)} \xi\delta \left\{\cos\theta\left[\Gamma_3 A e^{-\delta\alpha_1 z} + \Gamma_4 C e^{-\delta\alpha_2 z}\right] - \sin\theta\left[\mu\beta\delta E e^{-\beta\cdot\delta\cdot z}\right]\right\} d\xi d\theta \tag{30}$$

$$\sigma_{zy}(x,y,z,\omega) = \tfrac{1}{2\pi^2}\tfrac{1}{\sqrt{2\pi}} * \int_{-\pi/2}^{\pi/2}\int_{-\infty}^{\infty} \pi \cdot sign(\delta\xi)\, e^{i\delta\xi(x\cos\theta + y\sin\theta)} \xi\delta \left\{\sin\theta\left[\Gamma_3 A e^{-\delta\alpha_1 z} + \Gamma_4 C e^{-\delta\alpha_2 z}\right] + \cos\theta\left[\mu\beta\delta E e^{-\beta\cdot\delta\cdot z}\right]\right\} d\xi d\theta. \tag{31}$$

$$\sigma_{zz}(x,y,z,\omega) = \frac{1}{2\pi^2}\frac{1}{\sqrt{2\pi}} \int_{-\pi/2}^{\pi/2}\int_{-\infty}^{\infty} \pi \cdot sign(\delta\xi)\, e^{i\delta\xi(x\cos\theta + y\sin\theta)} \xi\delta \left\{\Gamma_1 A e^{-\delta\alpha_1 z} + \Gamma_2 C e^{-\delta\alpha_2 z}\right\} d\xi d\theta \tag{32}$$

Expressions (27) through (32) must be evaluated numerically. There are only three components of the stress tensor given in equations (30) to (32). The other three stress components may be obtained from the displacement equations. It should also be clear that the values of the constants A, C and $E$are to be taken from equations (24), (25) and (26).

5 Numerical Evaluation

Integrand behavior. All the integrands presented in equations (27) to (32) present a similar structure. The typical integrand shows a kernel $K(\xi)$ multiplied by oscillating functions $H(\xi, \theta)$. The kernels $K(\xi)$ of the elastic half-space present 3 singularities related to the compression, shear and Rayleigh waves [23]. These singularities may be smoothed by introducing damping coefficients at the imaginary part of the constitutive parameters μ and λ [23]. The integration strategy applied in this article can only be used in the viscoelastic case, in which the damping factor is present, $\eta > 0$. This leads to non-singular integrands. For the case of an elastic continua, in which $\eta = 0$, the resulting singular integrands must be regularized. The second part of the typical integrand consists of an oscillating term that will be named $H(\xi, \theta)$. It is to be evaluated in the range $-\pi/2 < \theta < +\pi/2$. The oscillation frequency of the integrand depends on the position of the field point (x, y), on the normalized wave number ξ and on geometry of the loading area (a, b). It can be shown that for increasing values of the wave number $\xi = \xi_0$, the integrand $H(\xi = \xi_0, \theta)$ becomes more difficult to integrate.

Integration strategy. The methodology applied to the numerical evaluation of expressions (27) through (32) is now described. For a given circular frequency ω, for a set of constitutive parameters ρ, μ, λ, η, for loading geometry a, b and for a given set of coordinates x, y, z the improper integration in the range $0 < \xi < +\infty$ is performed. Within this integration procedure, for every value of the normalized wave number $\xi = \xi_0$, the oscillating part of the integrand $H(\xi = \xi_0, \theta)$ is evaluated within the range $-\pi/2 < \theta < +\pi/2$.

For the oscillating part $H(\xi = \xi_0, \theta)$, the interval $-\pi/2 < \theta < +\pi/2$ is subdivided into a number of sub-intervals, *NI*. An empiric rule can be established regarding the initial number of sub-intervals to be used:

$$NI = \frac{|\delta\xi\,(x + y)\,|}{3} \tag{33}$$

The integration over these sub-intervals is performed with standard 2-points Gauss quadrature. In the sequence, a 4-points rule is applied and convergence is verified. If the desired accuracy is not achieved, a 6-points Gauss rule is applied. Numerical experience shows that, starting with the number of initial sub-intervals NI given in (33) and using the 6-points Gauss rule, an accuracy of 10^{-5} is usually achieved in the evaluation of the integrals, within each sub-interval. The improper integration over ξ is accomplished in two steps. Initially, a proper integration is performed using the Gauss rule within the range $0.0 < \xi < 1.5$. Interval sub-division strategy is applied until the required accuracy is obtained. For the remaining integration interval, $1.5 < \xi < +\infty$, a forward marching integration scheme has been devised. The interval length of the forward marching procedure $\Delta\xi$ is determined according to the empirical rule

$$\Delta\xi = \frac{\pi}{\sqrt{x^2 + y^2}\sqrt{\omega^2\rho}} \tag{34}$$

Every time a new interval $\Delta\xi$ is integrated, its result is compared to the accumulated value obtained in all previous stages. If the contribution of the last interval is smaller than a prescribed value the integration process stops. If this criterion is not fulfilled, the integration process marches on, over a new interval $\Delta\xi$.

6 Numerical results

The numerical results obtained in this work are compared to those obtained by Romanini [24] using the double Fourier integral transform. The parameters used in the numerical examples are: a=b=1m, ν=0.25, μ=1 N/m^2, ρ=1kg/m^3 and $\eta = 0.2$. A set of displacements for a frequency $\omega = 5$rad/s are given in figures 3 and 4. The components $U_{xx} = U_x(\sigma_{zx})$ and $U_{zx} = U_z(\sigma_{zx})$ are determined for a line inside the half-space, running in the x direction with coordinates $z = 1$m, $y = 0$m. Figure 5 reports a displacement component $U_{yx} = U_y(\sigma_{zx})$ for the circular frequency $\omega = 2$rad/s and for a line situated at the half-space surface, running in the x-direction with coordinates y=2m and z=0m. The results reported agree very well with those of Romanini [24]. In fact, the results obtained by the present methodology match so well those furnished by Romanini [24], so that they cannot graphically distinguished from each other. These perfect agreement in the numerical results allow us to think that the present formulation and implementation is correct.

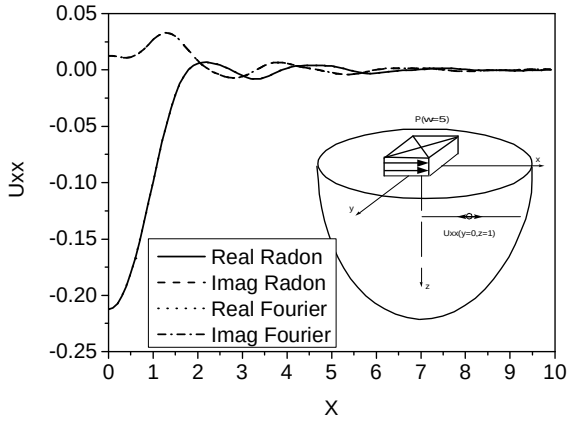

Figure 3: Displacement component U_{xx} for $\omega = 5$rad/s, y =0m , z =1m

7 Concluding remarks

Dynamic stationary displacement and stress fields for 3D viscoelastic half-spaces subjected to rectangular tangential loading of constant amplitude were determined by means of the double Radon-Fourier integral transforms. Internal damping was introduced by the elastic-viscoelastic correspondence principle. Calculations were performed for a frequency independent damping coefficient, reproducing the constant hysteretic damping model.

The numerical strategy used to perform numerically the inverse Fourier and Radon transforms was addressed. Validation of the proposed scheme was attempted by comparisons with solutions obtained

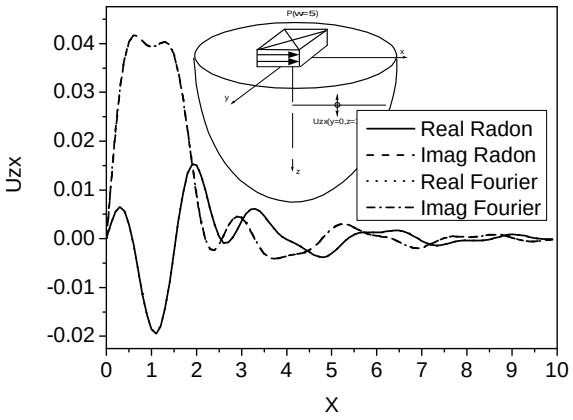

Figure 4: Displacement component U_{zx} for $\omega = 5$rad/s, y =0m , z =1m

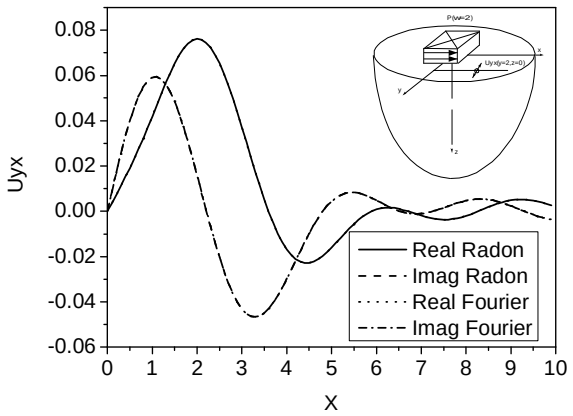

Figure 5: Displacement component U_{yx} for $\omega = 2$rad/s, y =2m , z =0m

by a double Fourier integral transform approach. Dynamic displacements fields within the half-space were compared to results obtained by a strategy based on the double Fourier integral transform. Accurate results were obtained by the proposed methodology. The mathematical structure stemming from the double Radon-Fourier transform strategy resembles the structure of the half-space surface problems solved using the double Fourier transform. A sample of original dynamic results, for displacement fields within the 3D half-space and at its surface, are furnished.

Acknowledgments

The research leading to this article has been supported by Fapesp, CNPq, Capes and FUNDECT-UFMS. This is gratefully acknowledged.

References

[1] Adolph, M., Mesquita, E., Carvalho, E.R. & Romanini, E., Numerically evaluated displacement and stress solutions for a 3d viscoelastic half-space subjected to a vertical distributed surface stress loading using the radon and fourier transforms. *Communications in Numerical Methods in Engineering*, **10.002/cnm932**. Published on line in Wiley Interscience - www.interscience.wiley.com.

[2] Sommerfeld, A., *Partial Differential Equations*. Academic Press: New York, 1949.

[3] Eringen, A.C. & Suhubi, E.S., *Elastodynamics*, volume 2. Academic Press: New York, 1979.

[4] Dominguez, J., *Boundary Elements in Dynamics*. Computational Mechanics Publications: Southampton, UK, 1993.

[5] Bettess, P., *Infinite Elements*. Penshaw Press, 1st edition, 1992.

[6] Rajapalske, R.K.N.D. & Karasudhi, P., Efficient elastodynamic infinte element. *International Journal of Solids and Structures*, **22(6)**, pp. 643–657, 1986.

[7] Givoli, D., *Numerical Methods for Problems in Infinite Domains*. Elsevier, 1992.

[8] Zavala, P.A.G., *Vibro-acoustic Analysis Using the Finite Element Method and the Dirichlet to Neumann Mapping*. Master's thesis, Faculty of Mechanical Engineering - State University at Campinas, UNICAMP, 1999. In Portuguese.

[9] Mesquita, E. & Pavanello, R., Numerical methods for the dynamics of unbounded domains. *Computational and Applied Mathematics*, **24(1)**, pp. 01–26, 2005.

[10] Beskos, D.E., Boundary element methods in dynamic analysis. *Applied Mechanics Reviews*, **40(1)**, pp. 01–23, 1987.

[11] Beskos, D.E., Boundary element methods in dynamic analysis: Part ii (1986-1996). *Applied Mechanics Reviews*, **50(3)**, pp. 149–197, 1997.

[12] Gaul, L., Dynamische wechselwirkung eines fundamentes mit dem viscoelastischen halbraum. *Ingenieur-Archiv*, **46**, pp. 401–422, 1977.

[13] Gaul, L., Dynamics of frame foundations interacting with soil. *Journal of Mechanical Design*, **102**, pp. 303–310, 1980.

[14] Rajapakse, R.K.N.D. & Wang, Y., Asce - green's functions for transversely isotropic elastic half space. *Journal of Engineering Mechanics*, **119(9)**, pp. 1724–1746, 1993.

[15] Barros, P.L.A. & Mesquita, E., Elastodynamic green's functions for orthotropic plane strain continua with inclined axis of symmetry. *International Journal for Solids and Structures*, **36**, pp. 4767–4788, 1999.

[16] Barros, P.L.A. & Mesquita, E., On the dynamic interaction and cross-interaction of 2d rigid structures with orthotropic elastic media possessing general principal axes orientation. *Meccanica*, **36(4)**, pp. 367–378, 2001.

[17] Deans, S.R., *Radon Transform and Some of Its Applications*. Krieger Publishing Company: Malabar: Florida, 1993.

[18] Wang, C.Y. & Achembach, J.D., (eds.), *Three-dimensional time-harmonic elastodynamic Green's functions for anisotropic solids*, volume 449 of *A-Mathematical and Physical Sciences*, Royal Society of London, 1995.

[19] Dravinski, N. & Niu, Y., Three-dimensional time-harmonic green's functions for a triclinic full-space using a symbolic computation. *International Journal for Numerical Methods in Engineering*, **53**, pp. 455–472, 2002.
[20] Georgiadis, H.G. & Lykotrafitis, G., A method based on the radon transform for three-dimensional elastodynamic problems of moving loads. *Journal of elasticity*, **65**, pp. 87–129, 2001.
[21] Adolph, M., *Synthesis of 3D Green's functions and auxiliary viscoelastic states using the Radon transform*. Ph.D. thesis, FEM/Unicamp, 2006. In Portuguese.
[22] Christensen, R.M., *Theory of Viscoelasticity*. Academic Press: New York, 1982.
[23] Graff, K., *Wave Motion in Elastic Solids*. Dover Publications: Ney York, 1991.
[24] Romanini, E., Mesquita, E. & Barros, R.M., On two strategies to synthesize influence functions for three-dimensional half-space problems. *14th ASCE Engineering Mechanics Conference*, 21-24 May, 2000. University of Texas, Austin, 5pp. (Proc. in CD-ROM).

Appendix A. Auxiliary equations

$$\psi_1 = \frac{\alpha_1^2 (\lambda + 2\mu) - \xi^2 \mu + 1}{i\xi (\lambda + \mu) \alpha_1} \tag{A1}$$

$$\psi_2 = \frac{\alpha_2^2 (\lambda + 2\mu) - \xi^2 \mu + 1}{i\xi (\lambda + \mu) \alpha_2} \tag{A2}$$

$$\Gamma_1 = -\alpha_1 (\lambda + 2\mu) + i\xi\lambda\psi_1 \tag{A3}$$

$$\Gamma_2 = -\alpha_2 (\lambda + 2\mu) + i\xi\lambda\psi_2 \tag{A4}$$

$$\Gamma_3 = i\mu\xi - \mu\alpha_1\psi_1 \tag{A5}$$

$$\Gamma_4 = i\mu\xi - \mu\alpha_2\psi_2 \tag{A6}$$